Chapter 10

Using Single-Molecule FRET to Evaluate DNA Nanodevices at Work

Nibedita Pal and Nils G. Walter

Abstract

The observation of DNA nanodevices at a single molecule (i.e., device) level and in real time provides rich information that is typically masked in ensemble measurements. Single-molecule fluorescence resonance energy transfer (smFRET) offers a means to directly follow dynamic conformational or compositional changes that DNA nanodevices undergo while operating, thereby retrieving insights critical for refining them toward optimal function. To be successful, smFRET measurements require careful execution and meticulous data analysis for robust statistics. Here we outline the elemental steps for smFRET experiments on DNA nanodevices, starting from microscope slide preparation for single-molecule observation to data acquisition and analysis.

Key words DNA nanotechnology, Fluorescence microscopy, FRET-based distance measurements, Single-molecule fluorescence resonance energy transfer, Surface immobilization

1 Introduction

The DNA duplex is inarguably one of the most fascinating examples of molecular self-assembly. Its programmability and structural predictability based on simple sequence-based rules are enabling the design of remarkable two- and three-dimensional structures with unprecedented molecular precision and diversity [1–7]. Structural DNA nanotechnology underwent a revolution when Paul Rothemund introduced "scaffolded DNA origami" wherein a long single-stranded DNA scaffold is folded intricately with the help of a large number of small staple strands segmentally complementary to the scaffold [2]. This pioneering work opened up entire new avenues for designing self-assembled DNA nanostructures. While from the very conception of DNA nanotechnology the design of intricate static DNA architectures has remained a focus, in recent years the engineering of nanoscale machines and actuated nanodevices has become increasingly popular. The strategies developed to power these nanodevices include strand displacement

Julián Valero (ed.), *DNA and RNA Origami: Methods and Protocols*, Methods in Molecular Biology, vol. 2639,
https://doi.org/10.1007/978-1-0716-3028-0_10,

through toehold exchange [8, 9]; the application of external stimuli such as ions [10], light [11], pH [12], etc.; or the exploitation of the catalytic activity of DNA [13, 14]. These DNA-based nanodevices have found interesting and versatile applications ranging from payload delivery [6] to biosensing of pH [15], ions [16], and enzymatic activity [17] across a living cell. Among the numerous DNA nanodevices designed so far, DNA walkers offer the prospect of cargo transport that simulates the function of biological motor proteins such as kinesin and myosin. One challenge in designing such walkers, or any other actuated DNA nanodevice, remains in their often-sluggish performance, taking significant time to perform just one operation. Recent advances have started to improve the design for faster translocation by cartwheeling [9] and transduction of external energy sources [18] to create DNA walkers of higher speed.

For the facile design of DNA nanodevices, several simulation software packages have been developed [19, 20]. Next, biochemical characterization and manipulation techniques are readily available to produce the DNA design. For example, restriction enzymes and ligases cut double-stranded DNA at specific sites and join the ends together, respectively [21–23]. Polymerase chain reaction (PCR) and cloning make it possible to generate DNA of a specific sequence in large quantity [24]. Long single-stranded DNA is commercially available as a scaffold strand in the form of M13 bacteriophage DNA [2, 4, 7] or can be generated by asymmetric PCR [25, 26]. Combining all these techniques makes it quite feasible to translate a computer-generated model of a DNA nanodevice into reality [27].

Once designed and synthesized, the characterization of DNA nanodevices remains a crucial step for advances in the field of DNA nanotechnology. Atomic force microscopy (AFM) is one of the standard tools with nanoscale spatial resolution and an ability to image under native conditions, albeit after firm adsorption to a mica mineral surface, that has been extensively applied to DNA nanodevices such as walkers [14, 28, 29]. Another important toolset entails either negative stain or cryogenic electron microscopy, which requires generating a thin layer of sample to be scanned by an electron beam in a vacuum [28, 29]. However, many DNA nanodevices require additional characterization to observe, ideally in real-time, dynamic events such as actuated shape changes or molecular locomotion. Here, bulk fluorescence spectroscopy offers a solution since it operates in real time and in solution under a broad set of native condition, is easy to detect and quantify, and is compatible with in situ manipulation such as the introduction of triggers and cofactors as well as with the use of microplates for parallelization and high-throughput screening [30].

DNA nanodevices often are actuated through conformational changes triggered by DNA strand displacement or changes in buffer additives. Fluorescence (or Förster) resonance energy transfer (FRET) offers a solution to observe in real time conformational changes between two judiciously placed fluorophores, which often proves critical toward understanding and optimizing functional performance [30, 31]. During FRET, the excitation energy of one fluorophore, the donor (e.g., Cyanine 3/Cy3), is non-radiatively transferred to the second fluorophore, or acceptor (e.g., Cyanine 5/Cy5), in a distance-dependent manner. As such, FRET enables one to monitor conformational changes in the 1–10-nm distance range that a DNA nanodevice undergoes during its operation. Importantly, modern single-molecule fluorescence microscopy has revolutionized how we perceive any molecular system as it reveals diversity of system behavior and malfunction [32, 33]. Single-molecule FRET (smFRET) of surface-immobilized DNA nanodevices allows us to monitor their actuation or locomotion over long periods of time when photobleaching and blinking of the fluorophores are minimized by removal of oxygen and speedy recovery from dark triplet states, respectively [34]. For example, smFRET has been employed recently for the real-time observation of the unidirectional rotation of a DNA nanoengine as an integral part of one of the fastest DNA walkers reported so far [18]. smFRET enabled the direct measurement of the rotation speed as an essential step in determining the nanoengine walking speed. Similarly, a recent application of smFRET to optimizing a cartwheeling DNA walker helped optimize its design parameters and thus its locomotion [9]. These examples show the synergistic interplay between design and characterization for optimizing the function of DNA nanodevices.

A total internal reflection fluorescence microscope (TIRFM) (*see* Fig. 1) is a powerful tool for smFRET detection with high signal-to-noise ratio [35]. In this chapter, we outline the steps necessary for efficient wide-field, camera-based, prism-type TIRFM for smFRET data acquisition, which allows one to image many single nanodevices simultaneously. We also describe general methodology for the analysis of smFRET data. As a representative example, we describe a DNA catenane-based nanoengine consisting of a catalytic stator that unidirectionally rotates against an interlocked rotor; a zinc finger protein fused to T7 RNA polymerase attached to the rotor harnesses the energy of NTP hydrolysis to fuel the continuous rotatory motion [18]. Although illustrated with this example, any fluorescently labeled nanodevice can be investigated using the smFRET protocols outlined here with only limited adjustments for specific needs. Similar protocols can be used for assays involving single-particle tracking [9] or single-molecule kinetic analysis of RNA transient structure (SiM-KARTS) strategies for monitoring nanodevice function [36]. Related super-resolution

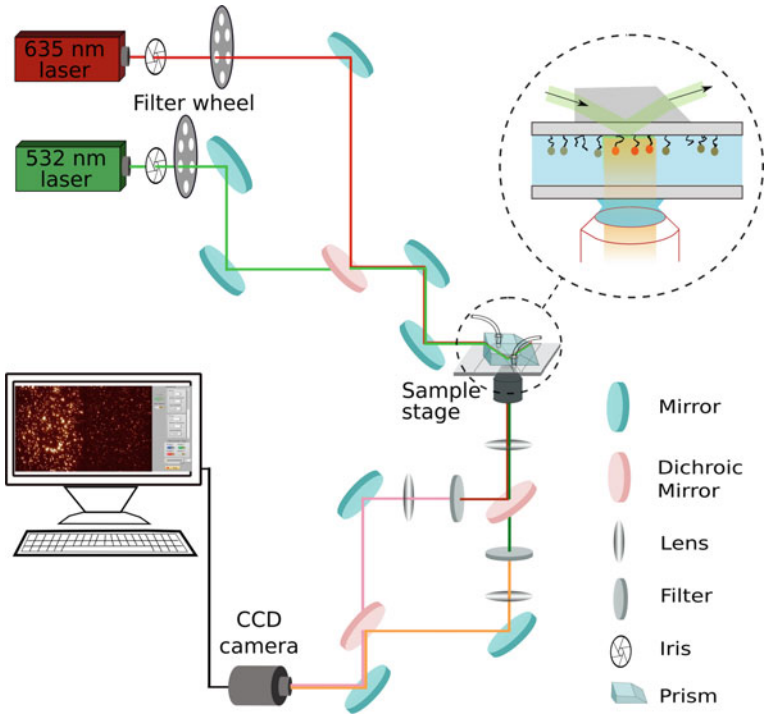

Fig. 1 Prism-type total internal reflection fluorescence microscope (TIRFM)

fluorescence techniques are another powerful toolset that can be used to monitor DNA nanodevice movement or compositional change over time, for the details of which the reader is referred to prior works [37, 38].

2 Materials

All solutions are prepared using autoclaved doubly deionized water (18 MΩ · cm at 25 °C). Chemicals are of highest commercially available purity and used without further purification.

2.1 Cleaning of Quartz Microscope Slides

1. Alconox.
2. Potassium hydroxide pellets (KOH).
3. Ammonium hydroxide.
4. Hydrogen peroxide.
5. Propane torch (14.1 OZ., Worthington).
6. Aqueous "base piranha": 20% v/v hydrogen peroxide, 20% v/v ammonium hydroxide, 60% v/v water.

2.2 Functionalization of Quartz Slide and Making Microfluidic Channel

1. Quartz microscope slide, 1 inch × 3 inches × 1 mm (G. Finkenbeiner).
2. Micro coverslip, rectangular, No. 1½, 24 × 30 mm.
3. 0.2″ ID × 0.6″ OD 100-80 microbore Tygon tubing (Cole-Parmer).
4. Double-sided sticky tape, ½″ wide.
5. Two-component epoxy resin (Double Bubble, Hardman Adhesives).
6. (3-Aminopropyl)triethoxysilane (APTES).
7. Acetone, HPLC grade.
8. Biotin-PEG-succinimidyl valerate (biotin-PEG-SVA, molecular weight 5000 Da) and methoxy-PEG-succinimidyl valerate (mPEG-SVA, molecular weight 5000 Da) (Laysan Bio Inc).
9. Biotinylated bovine serum albumin.
10. Disulfosuccinimidyl tartrate (Soltec Ventures).
11. Streptavidin.
12. Sodium bicarbonate.

2.3 Buffer Preparation (See Notes 1 and 2)

1. Trizma base, crystalline (≥99%).
2. Magnesium chloride hexahydrate ($MgCl_2$).
3. Sodium hydroxide pellets, anhydrous (NaOH).
4. Hydrochloric acid (HCl), 1 N.
5. Sodium chloride (NaCl, ≥99%).
6. Ethylenediaminetetraacetic acid (EDTA).
7. Acetic acid.
8. T50 buffer: 10 mM Tris-HCl, pH 8.0, 50 mM NaCl.
9. 1× TAE buffer: 40 mM Tris base, 20 mM acetic acid, pH 7.5, 1 mM EDTA.
10. 1× TAE-Mg^{2+} buffer: 40 mM Tris base, 20 mM acetic acid, pH 7.5, 12.5 mM $MgCl_2$, 1 mM EDTA.
11. 5× transcription buffer: 200 mM Tris–HCl, pH 7.9 at 25 °C, 50 mM DTT, 50 mM NaCl, and 10 mM spermidine.
12. Transcription mixture: rNTP set (2 mM each GTP, ATP, CTP, and UTP), 1× transcription buffer, 40 U RNasin ribonuclease inhibitor, 25 mM $MgCl_2$, 1× OSS, and 5% (v/v) DMSO.

2.4 Oxygen Scavenger System for smFRET Assay

1. Trolox (6-hydroxy-2,5,7,8-tetramethylchroman-2-carboxylic acid), 97% (Acros Organics).
2. Protocatechuate 3,4-dioxygenase from *Pseudomonas* sp. (PCD).
3. Protocatechuic acid (PCA).

4. Glycerol (≥99%).
5. 5 M KOH prepared in double distilled water.
6. PCD stock buffer: 100 mM Tris–HCl, pH 8.0, 50 mM KCl, 1 mM EDTA, and 50% (v/v) glycerol.
7. 1× OSS: 20 nM PCD, 5 mM PCA, and 2 mM Trolox.

2.5 Prism-Type Total Internal Reflection Fluorescence Microscopy

More detailed specifications of the opto-mechanical components required for assembling a prism-type TIRFM can be found somewhere else [35]. Briefly, the components required are as follows:

1. Continuous-wave 532 nm green laser (CrystalLaser, CL532-050-L, 50 mW).
2. Continuous-wave 635 nm red laser (Coherent CUBE, 635-25C, 25 mW).
3. Inverted fluorescence microscope (Olympus IX71).
4. Intensified charge-coupled device (I-CCD) camera (I-Pentamax, Princeton Instruments).
5. 60 × 1.2 NA water immersion objective (Olympus UPlanApo).
6. Pellin-Broca prism (Thorlabs).
7. Dichroic mirror (Chroma, cutoff 610 nm).
8. Neutral density variable filter (Edmund Industrial Optics).
9. Band-pass filter (HQ580/60 m, Chroma).
10. Long-pass filter (HQ655LP, Chroma).
11. Immersion oil, low fluorescence (Olympus).
12. Mirrors (protected silver mirror, 1″ diameter) and lenses (Plano-convex, BK7, AR coating, Thorlabs).
13. Vibration isolation optical table (ST-UT2, Newport).
14. Computer.

3 Methods

3.1 Cleaning of Quartz Microscope Slides

The quartz slides are surface functionalized following a standard protocol [37, 39]. Before surface functionalization, they are subjected to a thorough cleaning procedure, as follows:

1. Place the quartz microscope slides into the Coplin jar, and sonicate in water-alconox (100:1) mixture for 1 h.
2. Wash thoroughly with water to ensure that no residual detergent is left.
3. If the slides are being reused from prior experiments, they are manually rubbed with ethanol to get rid of residual glue and then thoroughly rinsed with water.

4. Sonicate the quartz slides in 1 M KOH for 20 min followed by thorough washing with water.
5. If the slides are being reused, flame the slides with a propane torch to burn off any residual contamination or glue.
7. Put the slides in aqueous "base piranha" and heat at 60–70 °C for 30 min.
8. Thoroughly rinse the slides with water and dry under nitrogen gas flow.

3.2 Surface Functionalization of Quartz Microscope Slides

After cleaning, the slides undergo surface functionalization. Before proceeding, ensure that the quartz slides are completely dry:

1. Incubate the quartz slides in 2% (v/v) 3-amino-propyltriethoxysilane (APTES) in acetone. After incubating for 20 min, sonicate for 1 min and incubate for an additional 10 min.
2. Wash the quartz slides thoroughly with water and dry under nitrogen flow.
3. Place the quartz slides in a clean pipette box, keeping the surface to be functionalized face up.
4. Prepare a 1:3 mixture of biotin-PEG-SVA and mPEG-SVA in freshly prepared 0.1 M sodium bicarbonate (*see* **Note 3**).
5. Centrifuge the mixture for 1 min at 10,000 rpm to remove any air bubbles.
6. Place 70 μL of the solution on the slide surface to be passivated, and then sandwich gently by placing a dried glass coverslip on top. Care is to be taken to ensure no air bubbles are trapped.
7. Incubate the slides at room temperature in a dark and moist environment for 3–4 h (or overnight for best results). Fill the bottom of the pipette box partially with water for overnight incubation.
8. Carefully disassemble the glass coverslip by sliding it off and disposing it in the proper waste.
9. Rinse the quartz slides thoroughly with water and dry under nitrogen flow.
10. Place the quartz slides back in the pipette box, keeping the functionalized surface face up.
11. Dissolve 12 mg sulfo-DST in 420 μL of a freshly prepared 1 M aqueous sodium bicarbonate solution. Centrifuge the solution at 10,000 rpm for 1 min to remove any air bubbles.
12. Place 70 μL of the solution on the PEG-functionalized surface of the slide and sandwich as before with a glass coverslip.
13. After 30 min of incubation in a moist environment, remove the glass coverslip by sliding it off and properly disposing of it.
14. Thoroughly rinse the slides with water and dry under nitrogen flow.

3.3 Assembling Microfluidic Sample Cells

For TIRFM experiments, a microfluidic sample cell is assembled on a PEG-functionalized quartz slide by following these steps (*see* Fig. 2):

1. For buffer exchange, drill holes into the quartz slide using a 1 mm diamond drill bit.
2. Place double-sided sticky tape diagonally on the PEGylated surface to make a channel of 5–6-mm width.
3. Gently place a dry and clean glass coverslip on top of the tape to complete the microfluidic channel. The surface of the coverslip can be PEGylated as described above for additional passivation.
4. Tightly seal the channel by gently pressing the coverslip with the help of a pipette tip over the entire area covering the double-sided tape.
5. Seal particularly the ends of the channel with epoxy resin.
6. Cut a 200 μL pipette tip at 8–9 mm from the tip. Affix that cut pipette tip to the holes with epoxy resin.
7. Attach Tygon tubing with epoxy glue to the pipette tips for constructing an inlet and an outlet for the microfluidic channel (*see* Fig. 2).

The complete sample chamber can be stored for 2–3 weeks in a dark environment at room temperature. For reuse, the quartz slides are boiled in water for 30 min or longer. Tape, cover glass, and adhesive are peeled off using a razor blade and the slides subjected to the above cleaning protocol.

3.4 Preparation of an Oxygen Scavenging System (OSS)

1. Prepare 1 μM PCD in PCD stock buffer.
2. Sterile filter (0.2 μm) and divide the PCD solution into 0.5 mL aliquots and store at −80 °C until needed.
3. Prepare 100 mM PCA in water aided by the dropwise addition of 5 M KOH. Adjust pH to ~8.3.
4. Sterile filter and divide the PCA solution into 1 mL aliquots. Store at −20 °C.
5. Dissolve Trolox in water to a final concentration of 100 mM. Slowly add 5 M KOH to aid dissolving Trolox. Vortex vigorously and check pH after each addition. Adjust pH to 10–11. Store at −20 °C until needed.
6. Prepare 1× OSS right before using it in a smFRET experiment.

3.5 Surface Immobilization of Single-DNA Nanodevices and smFRET Data Acquisition

In TIRFM, an evanescent wave is generated using either a quartz prism or the microscope objective itself. This evanescent wave illuminates surface-immobilized fluorescent molecules. In this chapter, we describe smFRET data acquisition using a prism-type TIRFM (*see* Fig. 1 and **Note 4**):

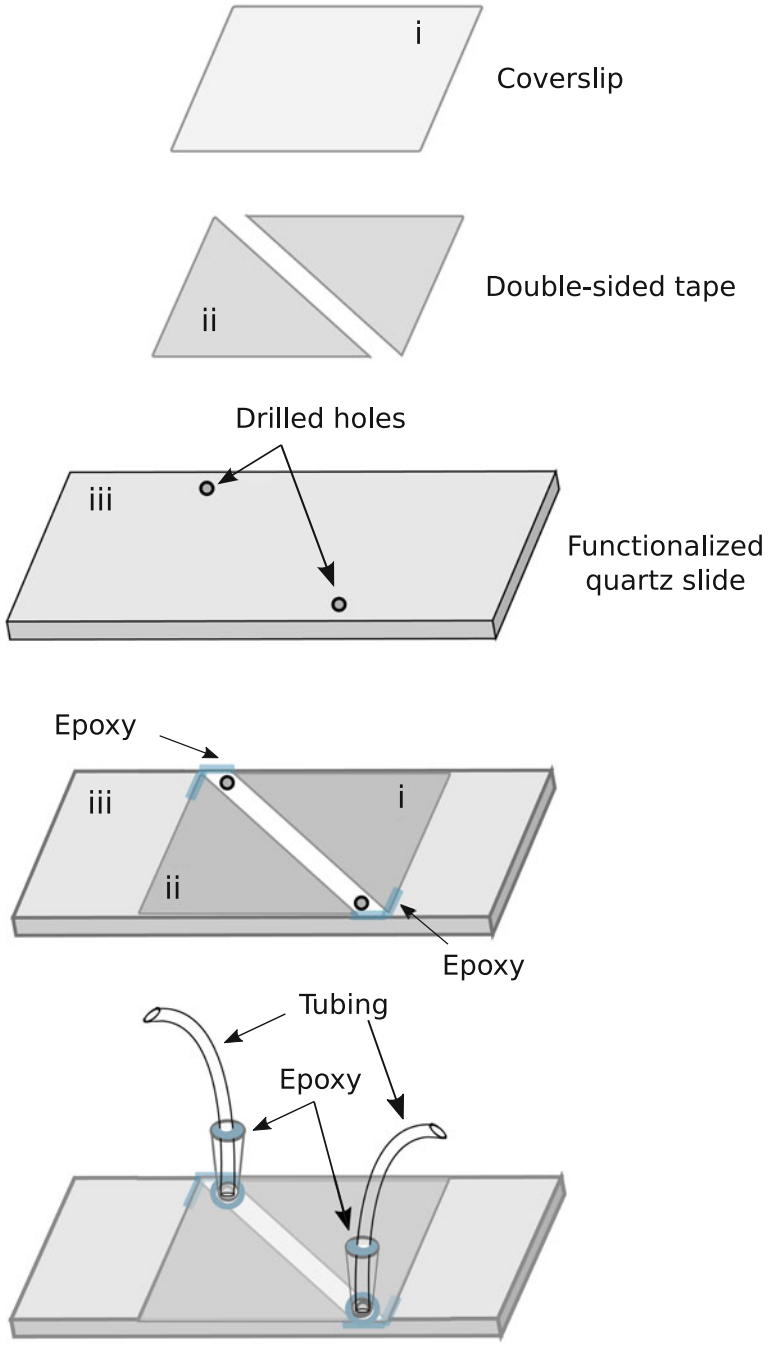

Fig. 2 Microfluidic channel assembly for single-molecule fluorescence microscopy

1. Rinse the microfluidic channel 2–3 times with ~200 μL T50 buffer.
2. Introduce 50 μL 0.2 mg/mL of streptavidin prepared in T50 buffer into the channel through the inlet tube, and incubate for 3–4 min.
3. Wash the channel with T50 buffer several times to flush out excess streptavidin. The slide surface within the channel is now ready to capture biotinylated DNA nanoengines or other biotinylated DNA nanodevices through a biotin-streptavidin interaction.
4. In the meantime, incubate the nanoengine with a threefold excess of T7 RNA polymerase-ZIF complex (T7RNAP-ZIF) (~0.6 nM:1.7 nM) at 37 °C for 30 min.
5. Add a drop of water onto the objective of the inverted microscope, and place the functionalized slide with the coverslip facing down onto the microscope stage held by an adapter plate.
6. Place a drop of immersion oil on top of the slide, and position the quartz prism carefully with the help of its holder.
7. Turn the 532 nm laser on at low power and adjust the objective focus to the glass-water interface.
8. Image the channel from one side to the other. Several bright spots often can be seen, indicating residual impurities. Photobleach these impurities using a high laser power that is compatible with the camera tolerance. Wash several times with 1× TAE buffer to expedite the photobleaching.
9. After removing the background, block the laser light with a shutter. Introduce ~100–300 μL of DNA nanodevices into the microfluidic chamber in the dark.
10. Briefly unblock the laser excitation and image using low excitation power. Several bright spots should be visible within the otherwise dark field of view. If the density of spots is sufficient, take the next step. If not, wait 3–4 min for more DNA nanodevices to bind to the surface. Alternatively or in addition, the concentration of the nanodevices can be increased. One may add 1× OSS in the solution in **step 9** to avoid photobleaching (*see* **Note 5**). However, a brief and low excitation power can avoid photobleaching.
11. Block the laser and wash away excess unbound catenane and T7RNAP-ZIF using 1× TAE-Mg^{2+} buffer.
12. Prepare enzymatic OSS at 1× concentration.
13. Prepare transcription mixture to relax the DNA double helix. Incubate on the slide for 3 min.
14. Seek a suitable field of view with a sufficient number of bright spots (*see* Fig. 3a).

15. Adjust the laser power to achieve a suitable signal-to-noise ratio while maintaining reasonably slow photobleaching.
16. Record fluorescence time traces in the form of movies for both donor and acceptor fluorophores using an I-CCD (or other single-molecule-sensitive camera) at the desired camera integration time. For example, to monitor the rotation of single nanoengines, we used 100 ms integration time. For our studies, the movie is saved in a data acquisition program written in MATLAB (scripts available upon request).
17. Either at the beginning or toward the end of the data acquisition, excite the acceptor fluorophore (Cy5 in our case) using the 638 nm red laser for a few frames to ensure the presence of acceptor (to distinguish from low-FRET states).
18. Repeat **steps 14–17** on different fields of view of the same slide to record a sufficient number of trajectories to achieve reliable statistics.

3.6 smFRET Data Analysis

The smFRET data collected as movies are typically analyzed using scripts written in MATALB or Interactive Data Language (IDL) (*see* **Note 6**):

1. Identify suitable molecules within the image that exhibit higher intensity than the surrounding pixels, and spatially match their signals in the donor and acceptor channels (Cy3 and Cy5 in our case (*see* **Note 7**)) (*see* Fig. 3a).
2. Extract time traces for the molecules identified using a suitable data analysis package. We use code written in the IDL package along with MATLAB scripts to extract and further analyze the trajectories (available upon request).
3. Set proper selection criteria. A significant signal-to-noise ratio, single-step photobleaching to reflect individual nanoengines, an acceptor intensity above a certain threshold, and other selection criteria can be applied, depending on the complexity of the trajectories. For our studies, we chose trajectories exhibiting an acceptor (Cy5) fluorescence intensity upon direct excitation well above background, anticorrelated donor (Cy3), and acceptor fluorescence intensities, as well as single-step photobleaching of both donor and acceptor. The FRET efficiency (E) at each time point is then calculated as $I_D/(I_A + I_D)$, where I_A and I_D are the apparent acceptor and donor fluorescence intensities, respectively (*see* Fig. 3b).
4. Generate a FRET efficiency histogram from the first 50 frames (or for the entire trajectory) of a sufficient number (typically >100) of trajectories, and fit it with a multi-peak Gaussian function as suitable to achieve low fit residuals (*see* Fig. 3c) [40]. The mean FRET value(s) represented by the center of

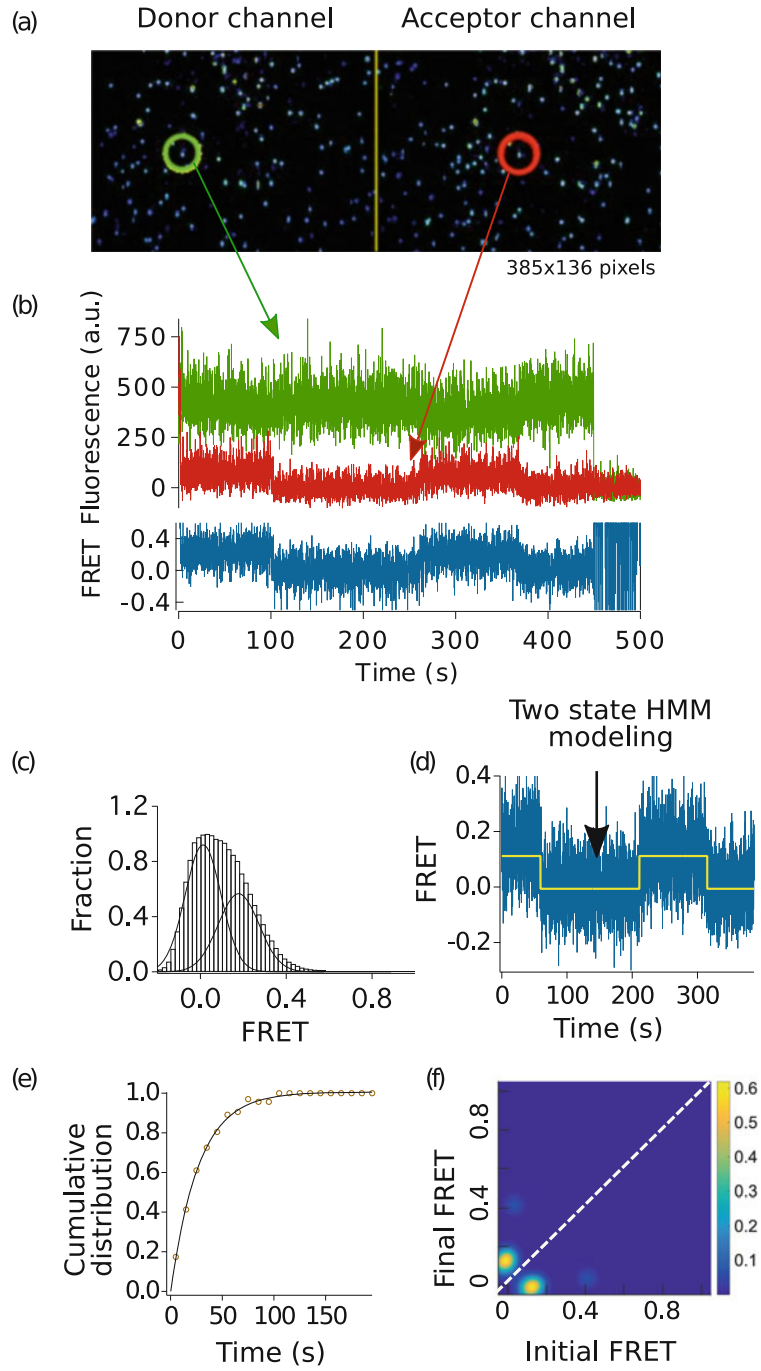

Fig. 3 smFRET data analysis steps of a DNA nanoengine [18] (**a**) Fluorescence signals from the fluorescently labeled nanoengines. (**b**) Extracted representative fluorescence intensity trajectories of donor (Cy3, green) and acceptor (Cy5, red) and corresponding FRET intensity trajectory (blue). (**c**) Single-molecule FRET efficiency histogram with multi-peak Gaussian fit. (**d**) Two-state hidden Markov (HMM) modeling of the FRET efficiency trajectory. (**e**) Cumulative dwell time distribution with suitable fit function. (**f**) Constructed transition occupancy density plot (TODP) from the idealized FRET trajectories

the peak(s) can be used to estimate the distance(s) between the fluorophores (R) using the following equation:

$E = \frac{1}{1+(R/R_0)^6}$, where R_0 is the Förster distance that is unique for a pair of donor and acceptor molecules; for Cy3 and Cy5, it is typically ~54 Å.

5. Fit the FRET intensity trajectories with proper idealizing models to extract the dwell times in the various FRET states. In the case of the nanoengine, we used two-state hidden Markov modeling, as implemented in the QuB package developed at the State University of New York at Buffalo, to extract the dwell times in the high- and low-FRET states (*see* Fig. 3d).
6. After idealization, extract the dwell times in each state for all trajectories.
7. Plot cumulative dwell time distributions, and fit them with suitable, often exponential, functions to extract the most probable dwell times using any suitable analysis software. For our purposes, we use OriginPro (*see* Fig. 3e).
8. From the idealized trajectories, construct the transition occupancy density plot (TODP) (*see* Fig. 3f). TODPs depict the fraction of molecules that populate a particular FRET state at least once, ensuring that fast transitions do not dominate this heat map [40]. Any population found on the diagonal represents static molecules (displaying no change in FRET state with time), whereas the off-diagonal population(s) represents dynamic molecules transitioning between FRET states during the observation time window (*see* Fig. 3d).

4 Conclusions and Future Outlook

In this chapter, we have illustrated a general procedure for how smFRET can be used as a technique to observe dynamic change in DNA nanodevices exemplified by a DNA catenane-based nanoengine. Application of smFRET of course is not limited to such comparably smaller structures of DNA nanodevices but additionally has been successfully employed investigating large, complex DNA origami-based nanodevices [28, 41–43]. These studies have demonstrated how the high temporal and spatial resolution offered by smFRET can be utilized to monitor origami-based DNA nanodevices whose response is often driven by conformational or compositional rearrangements triggered by environmental change. For example, smFRET measurements have been utilized to quantify depletion forces as low as ~100 fN in a DNA origami-based dynamic nanodevice [44]. Similarly, the mechanical properties of a DNA origami structure during voltage sensing can be monitored through smFRET signal intensity changes [41].

DNA origami-based nanostructures also have been used extensively as a canvas for functionalization with enzymes [7, 45], fluorescent dyes [46], DNA walkers [9], etc. with molecular scale precision. Single-molecule fluorescence microscopy has been used routinely as a technique to interrogate these systems, covering a broad spectrum of applications ranging from monitoring in real-time molecular kinetics [47, 48] and DNA walker locomotion [9] to enzyme catalytic activity inside a DNA cage [7]. However, the application of smFRET to monitoring conformational changes in the 3D structure of a DNA nanodevice during actuation is a relatively underexplored area and deserves more attention. As DNA nanodevices are becoming increasingly actuated, often going through intermediate configurations within sub-second time scales [49–51], the mapping of intra- and intermolecular distances in real time during dynamic actuation is becoming ever more important. Since smFRET provides a route to 3D distance triangulation by inclusion of multiple FRET pairs [51, 52], generally at the sub-second time scale [53], it can not only be used to complement existing characterization methods in DNA nanotechnology but also can open new possibilities for designing and optimizing rapidly actuated DNA origami of increasing size and complexity. Additionally, correlated measurements by combining several single-molecule techniques such as monitoring smFRET intensity while the DNA nanodevice is manipulated by atomic force microscopy (AFM) or optical tweezers, a detailed understanding of DNA nanodevice functionality in a complex environment can be achieved. Due to the necessary domain knowledge, implementing smFRET experiments for DNA nanodevices may appear a daunting barrier for newcomers to the field. Equipped with this protocol, however, we hope that scientists with little prior experience in single-molecule fluorescence microscopy will be able to adapt smFRET for their specific purposes.

5 Notes

1. Some of the reagents are potentially hazardous and should be handled with the manufacturer-prescribed precaution.
2. Freshly prepare all buffer solutions.
3. Biotin-PEG and mPEG should be stored at −20 °C and used within 6 months. Before opening the bottles, first warm them up to room temperature to avoid moisture condensation.
4. The steps described in this chapter follow the requirements for our DNA nanoengine [18] and DNA walker [9].
5. Sufficient care should be taken to protect the fluorescently labeled molecules from light during handling to prevent photobleaching. For example, dark Eppendorf tubes, aluminum foil wrapping, and low ambient light can be used for the purpose.

6. Numerous data analysis protocols have been developed for smFRET. In addition, good judgment should be used in interpreting all data to ensure that the conclusions are supported by the raw data.
7. Although Cy3 and Cy5 are used as FRET pair in our studies, different FRET pairs can be utilized instead. In that case, the excitation laser, dichroic filter, and emission filters need to be adjusted accordingly.

References

1. Winfree E, Liu F, Wenzler LA, Seeman NC (1998) Design and self-assembly of two-dimensional DNA crystals. Nature 394: 539–544
2. Rothemund PWK (2006) Folding DNA to create nanoscale shapes and patterns. Nature 440:297–302
3. Douglas SM, Dietz H, Liedl T et al (2009) Self-assembly of DNA into nanoscale three-dimensional shapes. Nature 459:414–418
4. Andersen ES, Dong M, Nielsen MM et al (2009) Self-assembly of a nanoscale DNA box with a controllable lid. Nature 459:73–76
5. Dietz H, Douglas SM, Shih WM (2009) Folding DNA into twisted and curved nanoscale shapes. Science 325:725–730
6. Douglas SM, Bachelet I, Church GM (2012) A logic-gated nanorobot for targeted transport of molecular payloads. Science 335:831–834
7. Zhao Z, Fu J, Dhakal S et al (2016) Nanocaged enzymes with enhanced catalytic activity and increased stability against protease digestion. Nat Commun 7:10619
8. Thubagere AJ, Li W, Johnson RF et al (2017) A cargo-sorting DNA robot. Science 357: eaan6558
9. Li J, Johnson-Buck A, Yang YR et al (2018) Exploring the speed limit of toehold exchange with a cartwheeling DNA acrobat. Nat Nanotechnol 13:723–729
10. Gerling T, Wagenbauer KF, Neuner AM, Dietz H (2015) Dynamic DNA devices and assemblies formed by shape-complementary, non--base pairing 3D components. Science 347: 1446–1452
11. You M, Chen Y, Zhang X et al (2012) An autonomous and controllable light-driven DNA walking device. Angew Chem Int Ed 51:2457–2460
12. Idili A, Vallée-Bélisle A, Ricci F (2014) Programmable pH-triggered DNA nanoswitches. J Am Chem Soc 136:5836–5839
13. Pei R, Taylor SK, Stefanovic D et al (2006) Behavior of polycatalytic assemblies in a substrate-displaying matrix. J Am Chem Soc 128:12693–12699
14. Lund K, Manzo AJ, Dabby N et al (2010) Molecular robots guided by prescriptive landscapes. Nature 465:206–210
15. Modi S, Swetha MG, Goswami D et al (2009) A DNA nanomachine that maps spatial and temporal pH changes inside living cells. Nat Nanotechnol 4:325–330
16. Saha S, Prakash V, Chakraborty K, Krishnan Y (2015) A pH-independent DNA nanodevice for quantifying chloride transport in organelles of living cells. Nat Nanotechnol 10:645–651
17. Dan K, Veetil AT, Chakraborty K, Krishnan Y (2019) DNA nanodevices map enzymatic activity in organelles. Nat Nanotechnol 14: 252–259
18. Valero J, Pal N, Dhakal S et al (2018) A bio-hybrid DNA rotor-stator nanoengine that moves along predefined tracks. Nat Nanotechnol 13:496–503
19. Castro CE, Kilchherr F, Kim D-N et al (2011) A primer to scaffolded DNA origami. Nat Methods 8:221–229
20. Douglas SM, Marblestone AH, Teerapittayanon S et al (2009) Rapid prototyping of 3D DNA-origami shapes with caDNAno. Nucleic Acids Res 37:5001–5006
21. Loenen WAM, Dryden DTF, Raleigh EA et al (2014) Highlights of the DNA cutters: a short history of the restriction enzymes. Nucleic Acids Res 42:3–19
22. Buckhout-White S, Person C, Medintz IL, Goldman ER (2018) Restriction enzymes as a target for DNA-based sensing and structural rearrangement. ACS Omega 3:495–502
23. Song IH, Shin SW, Park KS et al (2015) Enzyme-guided DNA sewing architecture. Sci Rep 5:1–9
24. Garibyan L, Avashia N (2013) Research techniques made simple: Polymerase Chain Reaction (PCR). J Invest Dermatol 133:20382

25. Veneziano R, Shepherd TR, Ratanalert S et al (2018) In vitro synthesis of gene-length single-stranded DNA. Sci Rep 8:1–7
26. Liu Q, Wang L, Frutos AG et al (2000) DNA computing on surfaces. Nature 403:175–179
27. Ke Y, Meyer T, Shih WM, Bellot G (2016) Regulation at a distance of biomolecular interactions using a DNA origami nanoactuator. Nat Commun 7:1–8
28. Birkedal V, Dong M, Golas MM et al (2011) Single molecule microscopy methods for the study of DNA origami structures. Microsc Res Tech 74:688–698
29. Jungmann R, Scheible M, Simmel FC (2012) Nanoscale imaging in DNA nanotechnology. Wiley Interdiscip Rev Nanomed Nanobiotechnol 4:66–81
30. Lakowicz JR (2006) Principles of fluorescence spectroscopy, 3rd edn. Springer, New York
31. Mao C, Sun W, Shen Z, Seeman NC (1999) A nanomechanical device based on the B-Z transition of DNA. Nature 397:144–146
32. Walter NG, Huang C, Manzo AJ, Sobhy MA (2008) Do-it-yourself guide: how to use the modern single-molecule toolkit. Nat Methods 5:475–489
33. Widom JR, Dhakal S, Heinicke LA, Walter NG (2014) Single-molecule tools for enzymology, structural biology, systems biology and nanotechnology: an update. Arch Toxicol 88:1965–1985
34. Aitken CE, Marshall RA, Puglisi JD (2008) An oxygen scavenging system for improvement of dye stability in single-molecule fluorescence experiments. Biophys J 94:1826–1835
35. Gibbs D, Kaur A, Megalathan A et al (2018) Build your own microscope: step-by-step guide for building a prism-based TIRF microscope. Methods Protoc 1:40
36. Rinaldi AJ, Lund PE, Blanco MR, Walter NG (2016) The Shine-Dalgarno sequence of riboswitch-regulated single mRNAs shows ligand-dependent accessibility bursts. Nat Commun 7:1–10
37. Michelotti N, de Silva C, Johnson-Buck AE et al (2010) A bird's eye view. Tracking slow nanometer-scale movements of single molecular nano-assemblies. Methods Enzymol 475: 121–148
38. Johnson-buck A, Nangreave J, Kim D et al (2013) Super-resolution fingerprinting detects chemical reactions and idiosyncrasies of single DNA pegboards. Nano Lett 13:728–733
39. Chandradoss SD, Haagsma AC, Lee YK et al (2014) Surface passivation for single-molecule protein studies. J Vis Exp 86:e50549
40. Blanco M, Walter NG (2010) Analysis of complex single-molecule FRET time trajectories. Methods Enzymol 472:153–178
41. Hemmig EA, Fitzgerald C, Maffeo C et al (2018) Optical voltage sensing using DNA origami. Nano Lett 18:1962–1971
42. Saccà B, Ishitsuka Y, Meyer R et al (2015) Reversible reconfiguration of DNA origami nanochambers monitored by single-molecule FRET. Angew Chem Int Ed 54:3592–3597
43. Li CY, Hemmig EA, Kong J et al (2015) Ionic conductivity, structural deformation, and programmable anisotropy of DNA origami in electric field. ACS Nano 9:1420–1433
44. Hudoba MW, Luo Y, Zacharias A et al (2017) Dynamic DNA origami device for measuring compressive depletion forces. ACS Nano 11: 6566–6573
45. Fu J, Liu M, Liu Y et al (2012) Interenzyme substrate diffusion for an enzyme cascade organized on spatially addressable DNA nanostructures. J Am Chem Soc 134:5516–5519
46. Stein IH, Steinhauer C, Tinnefeld P (2011) Single-molecule four-color FRET visualizes energy-transfer paths on DNA origami. J Am Chem Soc 133:4193–4195
47. Jungmann R, Steinhauer C, Scheible M et al (2010) Single-molecule kinetics and super-resolution microscopy by fluorescence imaging of transient binding on DNA origami. Nano Lett 10:4756–4761
48. Johnson-Buck A, Nangreave J, Jiang S et al (2013) Multifactorial modulation of binding and dissociation kinetics on two-dimensional DNA nanostructures. Nano Lett 13:2754–2759. https://doi.org/10.1021/nl400976s
49. Lauback S, Mattioli KR, Marras AE et al (2018) Real-time magnetic actuation of DNA nanodevices via modular integration with stiff micro-levers. Nat Commun 9:1446
50. Song J, Li Z, Wang P et al (2017) Reconfiguration of DNA molecular arrays driven by information relay. Science 357:371
51. Kopperger E, List J, Madhira S et al (2018) A self-assembled nanoscale robotic arm controlled by electric fields. Science 359:296–301
52. Hu J, Liu MH, Zhang CY (2019) Construction of tetrahedral DNA-quantum dot nanostructure with the integration of multistep Förster resonance energy transfer for multiplex enzymes assay. ACS Nano 13:7191–7201
53. Jeong C, Cho WK, Song KM et al (2011) MutS switches between two fundamentally distinct clamps during mismatch repair. Nat Struct Mol Biol 18:379–385